Title: Honeaite, a new gold-thallium-telluride from the Eastern Goldfields, Yilgarn Craton, Western Australia.

Running title: Honeaite, a new gold-thallium-telluride

Corresponding author: Clive M Rice, Department of Geology & Petroleum Geology, School of Geosciences, Meston Building, Kings College, University of Aberdeen, Aberdeen AB24 3UE, United Kingdom.

Email, c.rice@abdn.ac.uk
Phone, 44 1467 651218
Fax, no fax

Honeaite, a new gold-thallium-telluride from the Eastern Goldfields, Yilgarn Craton, Western Australia

Clive M Rice[1], Mark D Welch[2], John W Still[1], Alan J Criddle[†] & Chris J Stanley[2]

[1]Department of Geology & Petroleum Geology, School of Geosciences, Meston Building, Kings College, University of Aberdeen, Aberdeen AB24 3UE, United Kingdom.
[2]Department of Earth Sciences, Natural History Museum, Cromwell Road, London SW7 5BD, United Kingdom.
† *mortuus est* 2nd May 2002.
*E-mail: c.rice@abdn.ac.uk

Abstract

Honeaite, ideal formula Au_3TlTe_2, is a new mineral from the late Archaean Karonie gold deposit, Eastern Goldfields province, Western Australia. Honeaite is found with native gold, **(omission),** tellurobismuthite, petzite, hessite, calaverite, melonite, mattagamite, frohbergite, altaite, **(omission)**pyrrhotite and molybdenite. These minerals are concentrated in microvughs and microfractures mainly within areas of prehnite alteration of amphibolite. The mineralisation appears to have been deposited under greenschist facies conditions at lower temperatures than most gold deposits in the Eastern Goldfields.

Single-crystal X-ray studies identified the structure of honeaite as orthorhombic, space group *Pbcm*, with *a* = 8.9671 (4)Å, *b* = 8.8758(4) Å, *c* = 7.8419(5) Å, giving *V* = 624.14(6) Å^3 with *Z* = 4. The strongest reflections of the calculated powder X-ray diffraction pattern are [*d* in Å (I_{rel})(*hkl)*]: 2.938(100)(022), 2.905 (39,8)(322, 411), 2.989 (31)(300), 2.833 (23)(310), 1.853 (17)(332). Electron microprobe analysis (EDS mode) gave (wt%) Au 56.33, Tl 19.68, Te 24.30, total 100.31, leading to an empirical formula (based on **2 Te *apfu*) of $Au_{3.00}Tl_{1.01}Te_{2.00}$.** Honeaite is black with a metallic lustre and no observed cleavage. The calculated density is 11.18 g/cm^3. In reflected plane-polarized light it is slightly bluish grey. Between crossed polars it is weakly anisotropic with dark brown to dark blue rotation tints. Reflectance values in air and in oil are given.

Honeaite is named after the late Russell M. Honea (1929-2002). **Omission.**

KEYWORDS: Honeaite; new mineral; gold-thallium-telluride; Eastern Goldfields; Western Australia.

Introduction

Honeaite was discovered by the late Russell M. Honea in core from the Karonie gold deposit in the Eastern Goldfields of Western Australia at ~ 31°02’08”S (latitude), 122°33’39”E (longitude). He sent the samples containing what he believed to be a new Au-Tl-Te-bearing mineral to the late Richard A. Kosnar, a mineral dealer and owner of the company Mineral Classics located near Black Hawk, Colorado, USA. Kosnar passed them on to CMR in 1999. The chemistry and optics were determined at an early stage in the study and supported Honea`s suggestion that the mineral was new to science. However, completion of the study was delayed until the discovery in 2014 of grains large enough for a full structural analysis.

The Karonie deposit is on Cowarna Downs Station, which is 105 km east of Kalgoorlie and 7 km south of Karonie Siding on the Trans Australian Railway (Fig. 1.). It was initially managed by a joint venture between Freeport-McMoRan Australia Ltd., Karonie Gold N.L. and Golconda Minerals and later by Poseidon Gold Ltd.. Further exploration work has been carried out since (Jones 2007). Gold was produced from a series of open pits and some underground workings, with a total combined production of 4960 kg Au during the period 1987 to 1992 (Roberts et al. 2004).

It is appropriate to name the mineral in honour of the late Russell M Honea (1929-2002) who was a well-known mineralogist in the western USA and, indeed, globally. Russ Honea worked with some of the great mineralogists of the last century such as Cliff Frondel and Connie Hurlbut Jnr.. **He was initially a professor based at the University of Colorado, Boulder, Colorado, USA and later worked as an independent consulting geologist**. In addition to redefining the tellurides empressite and stuetzite (Honea, 1964) and describing several new minerals (e.g. billingsleyite, Frondel and Honea, 1968; chambersite, Honea and Beck, 1962) among his many publications, he also worked on the original description of the Karonie mineralogy for the mining company Freeport-McMoRan Inc.. He donated substantial numbers of specimens from his collection to the mineralogical museums of the University of Arizona and to Denver Museum of Nature and Science.

The mineral and name were approved by the Commission on New Minerals, Nomenclature and Classification of the International Mineralogical Association (IMA 2015-060). Holotype material is deposited in the collections of the Natural History Museum, London, catalogue number BM 2015, 36.

Honeaite appears to be identical to Unnamed Mineral 1993-27 Te:AuTl (Smith and Nickel, 2007). Chemical data for this unnamed mineral are given in Nechaev & Bondarenko (1993) and Bondarenko et al. (1993)**.** Nechaev & Cook (2000) describe Au_3TlTe_2 from the Maiskoe deposit, Ukraine while Bondarenko et al**.** (2005) describe Au_3TlTe_2 from the Potashnya deposit, Ukraine. The crystal structure of none of these phases was determined.

Regional geological setting of the Karonie gold deposits

The Karonie deposit occurs near the southeastern margin of the Eastern Goldfields Superterrane of the Archaean Yilgarn Craton (Fig. 1). The Superterrane is composed of a collage of fault-bounded, late Archaean (2.73-2.65 Ga) greenstone belts separated and intruded by extensive tracts of granitoid batholiths. It is divided into a number of terranes, which include the Kurnalpi terrane in which the Karonie deposit is located (Fig. 1) (Swager, 1997; Cassidy et al. 2006; Pawley et al. 2012). The Superterrane has had a complex tectonic history (eg Swager 1997; Blewett et al. 2010) and six stages of deformation have been distinguished by Blewett et al. (op cit). Regional metamorphic grades range from greenschist to amphibolite facies. Peak metamorphism coincided with D2 of Blewett et al. (2010) and was probably contemporaneous with the bulk of granite emplacement at c. 2.6Ga (Jones and Hall, 2004 and numerous references therein).

The Yilgarn Craton is famous for its gold deposits, most of which are found on the eastern side, the so-called Eastern Goldfields. The largest by far and a world class gold deposit is the Kalgoorlie Golden Mile (1500 t Au produced). Most of the gold is believed to have been emplaced during late transpressional events (D4 of Blewett et al. 2010), shortly before cratonization (Vielreicher et al. 2015). A final relatively minor stage of telluride-rich mineralization was controlled by strike-slip faulting (D5 of Blewett et al., 2010).

General Geology of the Karonie gold deposits

Karonie is located within the Murrin domain near the eastern margin of the Kurnalpi terrane (Fig. 1)(Cassidy et al. 2006; Jones 2007). The domain stratigraphy consists of a metamorphosed sequence of andesite-dominated volcanic and volcaniclastic rocks and interlayered metasediments, which were emplaced in an oceanic intra-arc setting (Barley et al. 2008). The deposits are about 3 km from the contact with the Erayinia Granitic Suite (Jones 2007).

The Karonie gold deposits lie within the north-trending Karonie shear zone which is over 100m wide. The gold deposits are predominantly hosted by quartz amphibolite and, in the northern part of the deposit, minor quartz-biotite-rich metasediments. The largest deposit, where honeaite was discovered, is the Main Zone orebody which has a strike length of about 600m and is about 40m wide (Fig. 2). It consists of several lenses that are generally conformable with the strike of the shear zone (Pigott and Green 1990; Poseidon Exploration Ltd., 1992; de Luca 1995; Roberts et al. 2004).

The metamorphic grade in the shear zone is mid to upper amphibolite facies whereas either side of the shear zone the grade decreases to greenschist facies actinolite-bearing rocks. There is intense ductile deformation in the shear zone and later brittle and brittle-ductile faults (de Luca 1995; Roberts et al., 2004). The two most accessible and informative accounts of the Karonie gold deposits are provided by de Luca (1995) and Roberts et al. (2004).

Gold mineralization

Four different types of alteration have been identified in the Karonie deposit (Roberts et al. 2004). In chronological order these are biotite-rich assemblages, mafic gneiss (coarsely banded hornblende-rich rocks), calc-silicate (thin pyroxene-rich veins with alteration selvedges in which hornblende has been replaced by diopside, plagioclase by epidote and ilmenite by titanite) and late alteration (biotite, calcic plagioclase and quartz) related to brittle-ductile faults (Roberts et al. 2004). In addition to the above, lower temperature alteration minerals including sericite, especially replacing feldspar, chlorite and prehnite are variably developed in all assemblages (de Luca 1995; Roberts et al. 2004).

Pigott and Green (1990) report a spatial association between gold mineralisation and calc silicate alteration, brittle-ductile faults and amphibolite/ metasediment contacts. However, Roberts et al (2004) report that the mineralization is found also in mafic gneiss and biotite-bearing mafic gneiss and that there is no consistent association with any rock type. In Figure 2 the mineralization forms a strike-parallel lense and is hosted by four rock types. De Luca (1995) noted the association of gold with low temperature minerals such as tellurides, epidote and prehnite.

Previous studies have reported that gold is the dominant component in clouds of fine grained ore minerals in hornblende and especially patches of epidote-clinozoisite and prehnite alteration (Pigott and Green, 1990; de Luca, 1995). Coarser gold occurs along fractures and cleavage planes in hornblende. Ore minerals associated with the gold are various Au-Ag-Ni-Pb-Bi-bearing tellurides, native Te and molybdenite (Pigott and Green 1990; de Luca 1995). Pigott and Green (1990) were the first to report an unnamed Tl telluride, undoubtably honeaite and discovered by Honea, who was a consultant at the mine. Up to 10% pyrrhotite, pyrite and chalcopyrite occurs in all rock types and is unrelated to gold mineralization.

Honeaite

Occurrence

The core samples containing honeaite came from borehole KD 41 at 78m, where the sequence is dominated by quartz amphibolite (Poseidon Exploration Ltd. 1992). The borehole was collared on section 10280N in the northern part of the Main Zone ore body (Fig. 2). Further honeaite-bearing material from the same core interval was provided by Ted Wilton (ex Exploration Manager-Western Australia for Freeport of Australia) and was included in this study. **In the following description of the occurrence of honeaite the compositions by electron microprobe of associated silicates and ore minerals are provided in Table 1.**

The host rock to the mineralization is a banded amphibolite with a primary assemblage consisting predominantly of randomly orientated sheaves of ferro-hornblende and mosaic textured calcic plagioclase (An 31) with small amounts of orientated ilmenite and pyrite and traces of zircon (**omission** Table 1).

Albitisation and calc-silicate alteration are widespread in the honeaite-bearing samples (Fig. 3A, B). Calcic plagioclase is replaced by more sodic plagioclase (An 10) along grain boundaries and in larger patches (**omission** Table 1). Sodic plagioclase commonly contains finely disseminated sericite.

Calc-silicate alteration includes actinolite, epidote, prehnite and titanite. Actinolite of variable iron content occurs as patches of alteration within and around the edges of hornblende (Fig.**4**; Table 1). Epidote and prehnite are widely developed as replacement products of hornblende and sodic plagioclase respectively (**Fig. 4, omission** Table 1). Prehnite also replaces epidote and cements fractures in epidote and mantles actinolite (Figs. **4, 5, omission**). There are small amounts of chlorite replacing hornblende and of apatite associated with epidote and prehnite. Late brittle fractures are filled by prehnite, sometimes with a little chlorite, and these may cut earlier prehnite (Fig. **6**). Titanite, like prehnite, also occurs as late brittle veins and as a replacement product of ilmenite (Figs. **5,6**).

Honeaite and other ore minerals, form clouds of small (largest c. 300 microns, most < 100 microns) inclusions roughly following the metamorphic banding (Fig**. 3**A). The mineralization also shows a broad spatial relationship with areas of epidote and prehnite alteration as noted by de Luca (1995) in a comprehensive study (Fig. **3**A). However, in detail the mineralization shows a much closer spatial relationship to areas of prehnite (Figs**. 6,7**). Given the small number of samples in our study we cannot say whether this is true of the deposit as a whole.

The inclusions consist mainly of gold (low Ag) and tellurobismuthite with small amounts of molybdenite, petzite, hessite, calaverite, melonite, mattagamite, frohbergite, altaite , pyrrhotite and honeaite. There are also composite grains of these minerals and honeaite, variously with gold, petzite, tellurobismuthite, molybdenite, chalcopyrite and pyrrhotite (Figs. **omission, 8, 9**)(Table 1). This mineral assemblage and its style are very close to that described from Karonie by Pigott and Green (1990) and de Luca (1995). Late cross-cutting prehnite veinlets contain a few grains of gold and a bismuth telluride but are largely barren (Fig. **6**). Small amounts of scheelite occur in a heavy mineral concentrate from the same core interval but it has not been observed in situ. It probably accounts for the W anomalies described in the deposit by de Luca (1995).

Over 25 honeaite grains were found occurring in microvughs and microfractures predominantly in prehnite with a few in epidote and hornblende (Figs. **9 to 13**). Honeaite morphology is determined by the shape of the vugh; no undoubted crystal faces were observed. The other tellurides and associated sulphides are also mainly vugh- and fracture-controlled within prehnite.

Appearance and physical properties

Honeaite is black with a metallic lustre and no observed cleavage. The calculated density is 11.18 g/cm^3. In plane-polarized incident light, honeaite is slightly bluish grey in colour (Figure **13**), very weakly bireflectant and very weakly pleochroic from grey (R_2) to slightly bluish grey (R_1). The mineral does not show any internal reflections. Between crossed polars, honeaite is weakly anisotropic with dark brown to dark blue rotation tints.

Reflectance data were obtained in air and in oil by the late Alan Criddle using the instrumentation and techniques described in Stanley et al (2002). The data are given in Table 2 and plotted in Figure **14**. Readings were taken for specimen and standard (WTiC) maintained under the same focus conditions.

Chemistry

Electron microprobe data were obtained on 17 grains of honeaite **(Table 3) omission**. These data were subsequently checked using a wavelength dispersive microprobe and suitable standards with excellent agreement between the datasets. The empirical formula (based on **2 Te a*pfu)* is $Au_{3.00}Tl_{1.01}Te_{2.00}$** giving a simplified formula of Au_3TlTe_2 which requires (wt%) Au 56.25, Tl 19.46 and Te 24.29, total 100.00.

Crystallography

Full details of the crystal structure of honeaite are reported elsewhere (Welch et al. submitted), so only a brief summary is given here. Honeaite is orthorhombic, space group *Pbcm*, with unit-cell parameters *a* 8.9671(4) Å, *b* 8.8758(4) Å, *c* 7.8419(5) Å, *V* = 624.14(6) Å^3 (*Z* = 4). The structure has been solved and refined using SHELX (Sheldrick, 2008) to final agreement indices R_1 = 0.033, wR_2 = 0.053**,** Goodness-of-Fit = 1.087, for full anisotropic refinement. The structure topology is completely novel and is composed of two components: (i) corrugated double-sheets of six-membered rings of corner-linked $TeAu_3$ pyramids, with Te and Au atoms located at apices, and Te having the one-sided three-fold coordination that is characteristic of a stereoactive lone-pair; there is additional intra-sheet connectivity *via* Au-Au bonds. (ii) rows of octahedrally-coordinated Tl atoms lying in the grooves of the corrugated sheets. Connections between adjacent $TeAu_3$ double-sheets involve only Tl-Au bonds. The structure is shown in Figure **15**. A CIF file containing data collection and structural information is deposited with the journal.

The crystals were too small to collect a quasi-Gandolfi `powder` pattern from a rotating single crystal and so the reflections were calculated based on the crystal structure (Table 4) .

The only compositionally similar Au-bearing phases of which we are aware are synthetic $CsAu_3S_2$, $RbAu_3Se_2$ and $CsAu_3Se_2$ (Klepp and Weithaler, 1996). The structure topology shared by these compounds is simple and consists of alternating planar sheets of $SeAu_3$ (SAu_3) pyramids and Cs (Rb) atoms, and is very different from the corrugated sheet of honeaite. Most importantly, the coordination of Se and S atoms is very different from Te in honeaite: Se and S are octahedrally-coordinated to three Au and three Cs (Rb) cations, e.g. Se[Au_3Cs_3] in $CsAu_3Se_2$.

One of the two non-equivalent Te atoms of honeaite has possible bonding distances to Tl, whereas the other Te is only bonded to Au. In both cases, Te[Au_3Tl_2] and Te[Au_3], the coordination is highly asymmetric (one-sided), suggesting stereoactivity of both Te atoms.

For $CsAu_3Se_2$ and $CsAu_3S_2$, the Cs-Se and Cs-S distances of 3.76 and 3.73 Å, respectively, imply that the Te(1)-Tl distance at 3.49 Å in honeaite is likely to be a bond, albeit contributing little bond valence to Te. Inclusion of much longer Te-Tl distances in honeaite (> 3.9 Å) are very unlikely to be bonds as they would result in very unusual coordination for Te. Thus, Tl can be considered to be octahedrally-coordinated. This coordination environment contrasts significantly with that of Cs and Rb in $CsAu_3S_2$, $RbAu_3Se_2$ and $CsAu_3Se_2$, in which they are octahedrally-coordinated by six Se (S) atoms.

The minerals petzite Ag_3AuTe_2 (Frueh, 1959) and fischesserite Ag_3AuSe_2 (Bindi and Cipriani, 2004) have the same 3:1:2 stoichiometry but very different structures from that of honeaite. Krennerite Au_3AgTe_8 (Dye and Smith, 2012) has $TeAu_3$ pyramids similar to those of honeaite, but less regular.

Discussion

Paragenetic position of honeaite

The earliest preserved mineral assemblage was formed during amphibolite facies metamorphism and is calcic plagioclase, hornblende and ilmenite **(omission)**. Ductile

deformation is recorded in the orientated ilmenite crystals whereas the randomly oriented sheaves of hornblende indicates continuing crystallization after ductile deformation ceased.

The nature and source of the hydrothermal fluids responsible for the subsequent alterations and mineralization are unknown but the changes from calcic to sodic plagioclase and hornblende to actinolite to prehnite reflect falling temperatures and a transition from amphibolite to greenschist and perhaps sub-greenschist facies conditions (Fig. **16**). The presence of late brittle prehnite-bearing microfractures shows that these mineralogical changes were accompanied by a change from ductile to brittle deformation, also seen at the deposit scale by late brittle faults.

The mineralization is intimately connected with the period during which prehnite was deposited since 1. the clouds of ore minerals are largely restricted to microfractures and vughs in areas of groundmass prehnite and 2.it postdates this prehnite but predates the final essentially barren cross-cutting prehnite veinlets. Thus, it was deposited from fluids related to the final stages of calc-silicate hydrothermal alteration, which may explain why the deposit scale relationship between all phases of calc-silicate alteration and mineralization is not closer (Fig. 2). The proposed late appearance of the mineralization is not incompatible with other studies that have described it occurring in earlier alteration phases at Karonie (Roberts et al. 2004), since in places these later ore fluids may have migrated **outside** the calc-silicate envelope.

The close spatial association of honeaite with gold and the other tellurides and especially the presence of composite grains indicate that honeaite is coeval with the rest of the mineralization. The presence of honeaite is further evidence for low temperature conditions since thallium-bearing minerals are typically found in low temperature hydrothermal systems such as Carlin-type gold deposits (Dickson et al. 1979; Cline et al. 2005. The combination of the style of mineralization (vugh- and fracture-hosted) and the associated mineral assemblage all suggest greenschist/ sub-greenschist rather than amphibolite facies conditions and emplacement at relatively shallow crustal levels.

While our limited study clearly points towards deposition of the observed mineralization at relatively low temperatures as noted by de Luca (1995), it may have been remobilised from earlier higher temperature deposits in the Karonie shear zone (Roberts et al. 2004; Jones and Hall 2004).

Comparisons with other telluride-bearing deposits in the Eastern Goldfields and classification of the mineralisation.

The Karonie deposit is one of several gold deposits in the Eastern Goldfields, which contain telluride mineralization that is late tectonic and post peak metamorphism and emplaced in brittle structures. Examples include Sunrise Dam (Baker et al. 2010), Mt Charlotte and Golden Mile (Mueller and Muhling 2013) and Bellerophon Nelson (Xue and Campbell 2014).

However, the close association of the gold and telluride mineralization at Karonie with low temperature calc-silicate (prehnite) alteration appears to be unique.

The Karonie deposit together with most other lode gold deposits in the Eastern Goldfields may be described as an orogenic gold deposit (Goldfarb et al. 2005). Despite the high metamorphic grade (amphibolite) of the host rocks the association of the gold and telluride mineralization at Karonie with brittle structures, vughs and prehnite alteration would place it towards the upper rather than lower crustal end member of the Continuum Model for orogenic gold deposits (Groves 1993). The transition from high temperature (amphibolite facies) to low temperature (greenschist facies) mineral assemblages could be explained by rapid late orogenic exhumation accompanied by reactivation of the Karonie shear zone (Groves et al. 1987; Vielreicher et al. 2015).

Acknowledgements

Ted Wilton (Radium Trail Geoscience, Nevada, USA**)(words omitted)** for providing additional core samples containing honeaite. Jenny Johnston (School of Geosciences, University of Aberdeen) for diagrams.

An anonymous reviewer for alerting us to the existence of some synthetic compounds which have an analogous stoichiometry to honeaite.

CJS acknowledges Natural Environment Research Council grant NE/M010848/1 Tellurium and Selenium Cycling and Supply.

References

Baker T., Bertelli M., Blenkinsop T., Cleverley J.S., McLellan, Nugus M. & Gillen D. (2010): P-T-X Conditions of Fluids in the Sunrise Dam Gold Deposit, Western Australia, and Implications for the Interplay between Deformation and Fluids. *Economic Geology*, 105, 873-894.

Barley, M.E., Brown, S.J.A., Krapez, B. & Kositcin, N. (2008): Physical volcanology and geochemistry of a Late Archaean volcanic arc: Kurnalpi and Gindalbie Terranes, Eastern Goldfields Superterrane, Western Australia. *Precambrian Research*, 161, 53-76.

Bindi, L. & Cipriani, C. (2004): Structural and physical properties of fischesserite, a rare gold-silver selenide from the de Lamar Mine, Owyhee County, Idaho, USA. *Canadian Mineralogist*, 42, 1733-1737.

Blewett, R.S., Czarnota, K., Henson, P.A. & Champion, D.C. (2010): Structural-event framework for the eastern Yilgarn Craton, Western Australia, and its implications for orogenic gold. *Precambrian Research*, 183, 203-229.

Bondarenko, S., Grinchenko, O. & Semka, V. (2005): Au-Ag-Te-Se mineralization in the Potashnya gold deposit, Kocherov tectonic zone, Ukrainian Shield. *Geochemistry, Mineralogy and Petrology,* **43,** 20-25.

Bondarenko, S. N., Nechaev, S. V. & Syroedov, N. F. (1993): Telluride mineral associations in the Maiskoe gold ore deposit (Ukrainian Shield). *Geologicheskii Zhurnal (1993) ,*No.5**,** 30-35 (in Russian).

Cassidy, K.F., Champion, D.C., Krapez, B., Barley, M.E., Brown, S.J.A., Blewett, R.S., Groenewald, P.B. & Tyler, I.M. (2006): A revised geological framework for the Yilgarn Craton, Western Australia. *Geological Survey of Western Australia*. Record 2006/8, 8pp.

Cline, J.S., Hofstra, A.H., Muntean, J.L., Tosdal, R.M. & Hickey, K.A. (2005): Carlin-Type Gold Deposits in Nevada: Critical Geologic Characteristics and Viable Models. *Economic Geology 100th Anniversary Volume*, 451-484.

De Luca, K.E. (1995): Gold mineralization in the Karonie greenstone belt, Eastern Goldfields, Western Australia. *Western Australian School of Mines*, MSc thesis (unpublished**). 174p.**

Dickson, F.W., Radtke, A.S. & Peterson, J.A. (1979): Ellisite, Tl2AsS3, a new mineral from the Carlin gold deposit, Nevada, and associated sulfide and sulfosalt minerals. *American Mineralogist*, 64, 701-707.

Dye, M.D. & Smyth, J.R. (2012): The crystal structure and genesis of krennerite, Au_3AgTe_8. *Canadian Mineralogist*, 50, 119-127.

Frondel, C. & Honea, R. M. (1968): Billingsleyite, a new silver sulfosalt. *American Mineralogist,* 53, 1791-1798.

Frueh, A.J. (1959): The crystallography of petzite, Ag_3AuTe_2. *American Mineralogist*, 44, 693-701.

Goldfarb, R.J., Baker, T., Dube, B., Groves, D.I., Hart, C.J.R., Robert, F. & Gosselin, P. (2005): World distribution, productivity, character, and genesis of gold deposits in metamorphic terranes. *Economic Geology 100th Anniversary Volume*, 407-450.

Groves, D.I., Phillips, GN, Ho, S.E., Houstoun, S.M. & Standing, C.A. (1987): Craton scale distribution of Archean greenstone gold deposits: predictive capacity of the metamorphic model. *Economic Geology*, 82, 2045-2058.

Groves, D.I. (1993): The crustal continuum model for late-Archaean lode-gold deposits of the Yilgarn Block, Western Australia. *Mineralium Deposita*, 28, 366-374.

Honea, R. M. (1964): Empressite and stuetzite redefined. *American Mineralogist,* 49, 325-338.

Honea, R. M. & Beck, F. R. (1962): Chambersite, a new mineral. *American Mineralogist,* 47, 665–671.

Jones, S.A. & Hall, C.E. (2004): Archaean and Protorozoic geology of the southeastern margin of the Yilgarn craton-A field guide. *Western Australia Geological Survey*, Record 2004/18, 37p.

Jones, S.A. (2007): Geology of the Erayinia 1:100 000 sheet. *Western Australia Geological Survey,* 1: 100 000 Geological Series Explanatory Notes, 37p.

Klepp K.O., Weithaler C. (1996): The crystal structures of $CsAu_3S_2$, $RbAu_3Se_2$ and $CsAu_3Se_2$ and their relationship to the $CsCu_3S_2$ structure type. *Journal of Alloys and Compounds*, 243, 1-5.

Ref omitted

Mueller, A.G. & Muhling, J.R. (2013): Silver-rich telluride mineralization at Mount Charlotte and Au-Ag zonation in the giant Golden Mile deposit, Kalgoorlie, Western Australia. *Mineralium Deposita*, 48, 295-311.

Nechaev, S. V. & Bondarenko, S. N. (1993): Thallium minerals of the Ukrainian Shield. *Mineralogicheskii Zhurnal,* 15 (1), 75-80 (in Russian).

Nechaev, S. V. & Cook, N. J. (2000): A natural occurrence of Au_3TlTe_2 from the Maiskoe Au deposit, Ukraine. *Neues Jahrbuch für Mineralogie Monatshefte,* 12**,** 557-562.

Pawley, M.J., Wingate, M.T.D., Kirkland, C.L., Wyche, S., Hall, C.E., Romano, S.S. & Doublier, M.P. (2012): Adding pieces to the puzzle: episodic crustal growth and a new terrane in the northeast Yilgarn Craton, Western Australia. *Australian Journal of Earth Sciences*, 59, 603- 623.

Pigott, G.F. & Green, N.P. (1990): Karonie gold deposit. *In* ``Geology of the mineral deposits of Australia and Papua New Guinea`` (Hughes F.E., ed.) *Australian Institute of Mining and Metallurgy*, Monograph 14, 531-535.

POSEIDON EXPLORATION LTD. (1992): Annual report. *Western Australia Geological Survey*, Statutory mineral exploration report, Item 11665, A35404 (unpublished). **136p.**

Roberts, F.I., Witt, W.K. & Westaway, J. (2004): Gold mineralisation in the Edjudina-Kanowna region, Eastern Goldfields, Western Australia. *Western Australian Geological Survey*, Report 90, 263p.

Sheldrick, G.M. (2008): A short history of SHELX. *Acta Crystallographica*, A64, 112-122.

Smith, D.G.W. & Nickel, E.H. (2007): A system for codification for unnamed minerals. report of the Subcommittee for Unnamed Minerals of the IMA Commission on New Minerals, Nomenclature and Classification. *Canadian Mineralogist*, 45, 983–1055.

Stanley, C.J., Criddle, A.J., Foerster, H-J & Roberts, A.C. (2002): Tischendorfite, $Pd_8Hg_3Se_9$, a new mineral from Tilkerode, Harz Mountains, Germany. *Canadian Mineralogist,* 40, 739-745.

Swager, C.P. (1997): Tectono-stratigraphy of late Archaean greenstone terranes in the southern Eastern Goldfields, Western Australia. *Precambrian Research*, 83, 11-42.

Vielreicher, N., Groves, G., McNaughton, N. & Fletcher, I. (2015): The timing of gold mineralization across the eastern Yilgarn craton using U-Pb geochronology of hydrothermal phosphate minerals. *Mineralium Deposita*, 50, 391-429.

Welch, M.D., Still, J.W., Rice, C.M. & Stanley, C.J. (Submitted): A new gold telluride structure topology: the crystal structure of honeaite Au_3TlTe_2.

Ref omitted

Ref omitted

Xue, Y. & Campbell, I. (2014): The mineralogy of the Bellerophon-Nelson telluride-bearing gold deposit, St. Ives camp, Yilgarn craton, Western Australia. *Canadian Mineralogist*, 52, 981-1006.

Figure captions

1. Regional location of the Karonie gold deposit.
2. Geological map of the Karonie Main Zone gold deposit at the 275m level (simplified and taken from Roberts et al., 2004, after Poseidon Exploration Ltd., 1992
3. A. False colour image of polished thin section of ore **sample KD 41/78**. Orange = epidote + prehnite; blue = plagioclase feldspar, mainly sodic plagioclase; green = hornblende; white specks = ore minerals. Metamorphic banding east-west. NW-SE veinlets are prehnite only. B. Same section normal colour, green = mainly hornblende, white = prehnite + epidote.
4. BSEM image (KD 41 78m)(4/21) Hornblende being replaced by epidote and actinolite (two generations, dark=actinolite, light= ferro-actinolite). Prehnite mantling

actinolite and filling cavities left by dissolution of plagioclase? Gold (white) occurring in cavities and fractures.

5. BSEM image (KD 41 78m)(4/20) Prehnite filling fractures in epidote. Gold hosted by prehnite. Ilmenite partially replaced by titanite.
6. BSEM image (KD 41 78m)(4/23) Late prehnite occurring in a brittle fracture cutting early prehnite and hornblende. The early prehnite contains numerous small white inclusions of a gold telluride (AuTe), whereas the late prehnite vein is barren. Ilmenite is altered to titanite.
7. BSEM image (KD 41 78m)(7/9) Typical `cloud`of mineralization hosted by prehnite, which is replacing plagioclase. The white inclusions are mainly gold and tellurobismuthite (BiTe).
8. BSEM image (KD 41 78m)(12/2) Composite grain of gold, a bismuth telluride and a nickel cobalt telluride hosted by prehnite. **PbTe = a lead telluride**.
9. BSEM image (KD 41 78m)(1/11A) Composite grain of honeaite, a bismuth telluride and gold hosted by prehnite.
10. BSEM image (KD 41 78m)(4/1) Honeaite in vugh within prehnite.
11. BSEM image (KD 41 78m)(4/8) Honeaite partially filling cavity in prehnite with a bismuth telluride (BiTe). Gold occurs in a fracture partially exploited by honeaite.
12. BSEM image (KD 41 78m)(4/14) Honeaite occurring in cavity in **zoned** prehnite.
13. Reflected light digital image of honeaite (bluish grey)**(same honeaite grain as in fig. 12)**, gold (yellow) and pyrrhotite(brownish-pink) in a gangue of prehnite.
14. Reflectance spectra for honeaite
15. Crystal structure of honeaite. **(a)** A single corrugated sheet of corner-linked $TeAu_3$ pyramids comprising six-membered rings. **(b)** Full structure showing two double- sheets with $TeAu_3$, pyramids shown in grey. Thallium atoms (green) occur in grooves in the corrugated sheets. The unit-cell projection is shown as a dotted red line. **(c)** Thallium coordination environment in which there are three Tl-Au intra-sheet bonds and a single Tl-Au inter-sheet bond (blue Au label). There are two long Tl···Te intra-sheet distances (dotted lines) that may not be genuine bonds. Numbers are bond distances in Å. **(d)** Ball-and-spoke representation of (b) showing intra-sheet Au-Au bonds (solid blue lines), Tl-Au bonds (black dashed lines) and Tl···Te distances (dashed red lines).
16. **The paragenesis** of honeaite

Tables

1. Electron microprobe analyses of Karonie silicates, gold and tellurides.

Footnote: The analyses were carried out using a MICROSCAN MK5 in energy dispersive mode (Link Analytical AN10/25S). The instrumental conditions were: accelerating voltage 15kV, current 2.8 nA, beam diameter c. 5 microns, take off angle 75 degrees and livetime 200 seconds. The standards used are a mixture of natural minerals, metal oxides and pure metals.

2. Reflectance data in air and in oil for honeaite. (COM refers to the Commission on Ore Mineralogy recommended minimum wavelengths)

3. Electron microprobe analyses (n=17) of honeaite.

Footnote: Standards used for honeaite: Au = Au metal; Tl = Thallium iodide; Te = Te metal. Instrument and operating conditions in Table 1.

4. Calculated powder XRD pattern of honeaite. Only reflections with relative intensities ≥ 5% are shown.

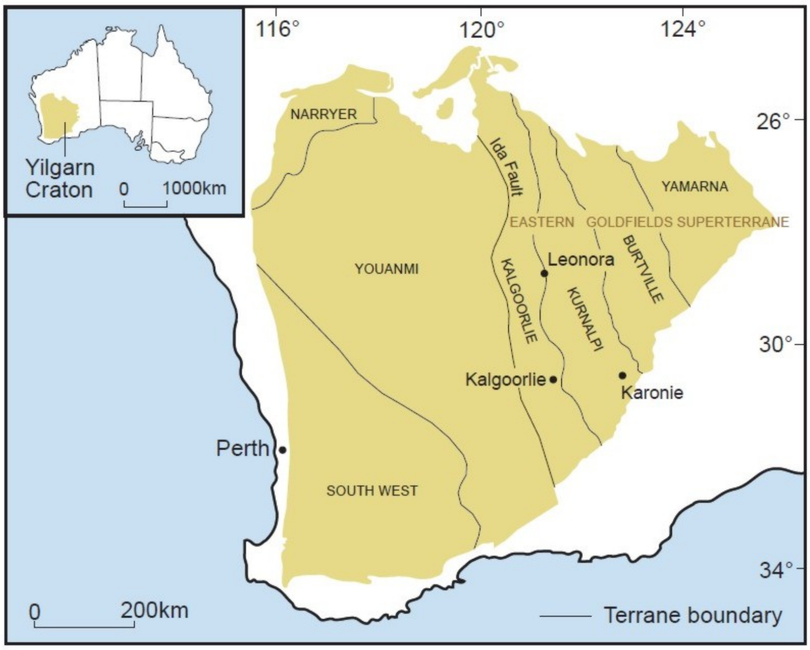

Fig. 1. Regional location of the Karonie gold deposit.

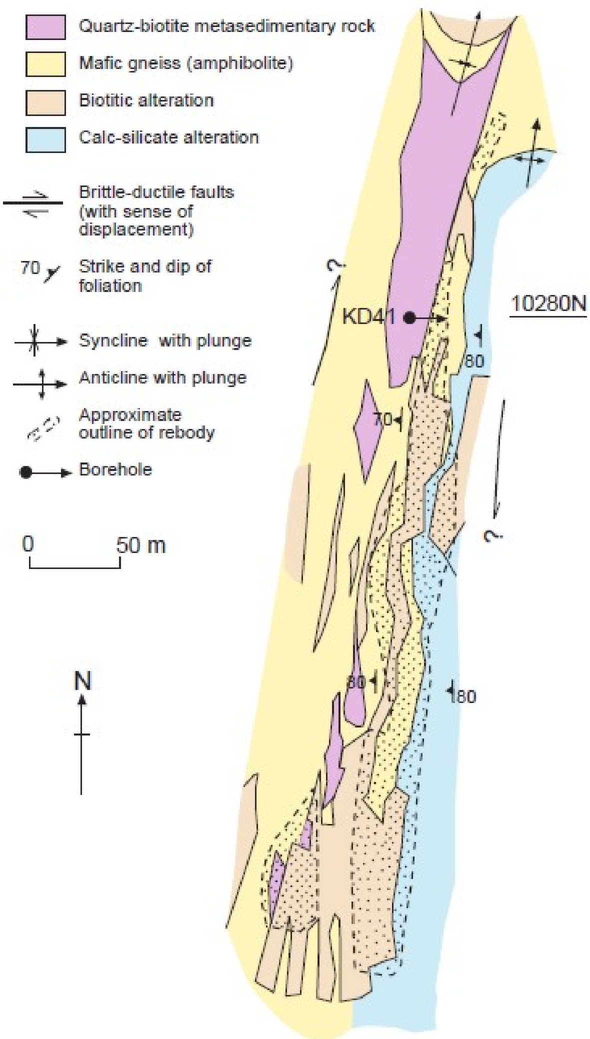

Fig. 2. Geological map of the Karonie Main Zone gold deposit at the 275m level (simplified and taken from Roberts et al., 2004, after Poseidon Exploration Ltd., 1992)

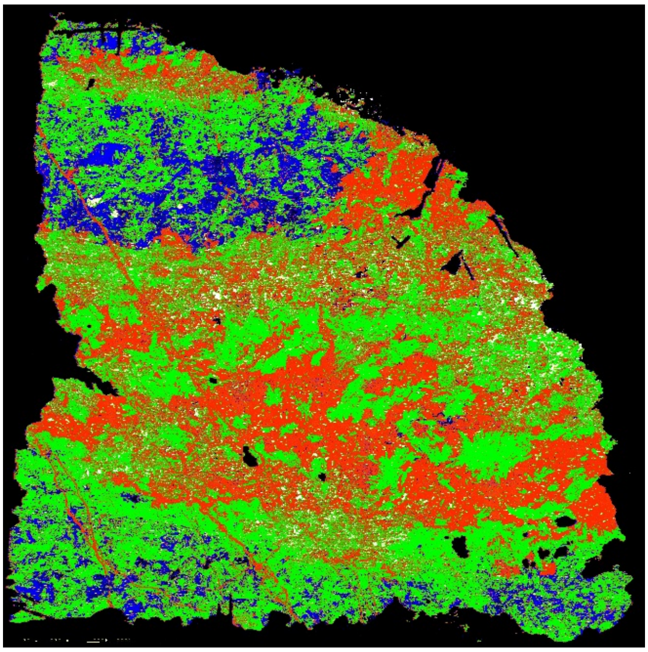

A

B

Fig.3. A. False colour image of polished thin section of ore **sample KD 41/78**. Orange = epidote + prehnite; blue = plagioclase feldspar, mainly sodic plagioclase; green = hornblende; white specks = ore minerals. Metamorphic banding east-west. NW-SE veinlets are prehnite only. B. Same section normal colour, green = mainly hornblende, white = prehnite + epidote.

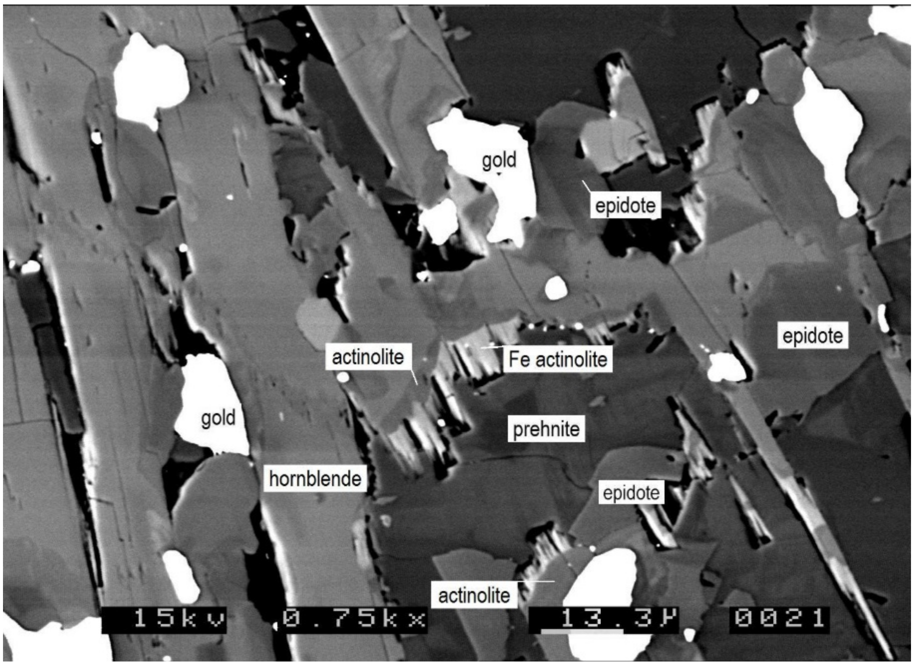

Fig. 4. BSEM image (KD 41 78m) (4/21) Hornblende being replaced by epidote and actinolite (two generations, dark=actinolite, light= ferro-actinolite). Prehnite mantling actinolite and filling cavities left by dissolution of plagioclase? Gold (white) occurring in cavities and fractures.

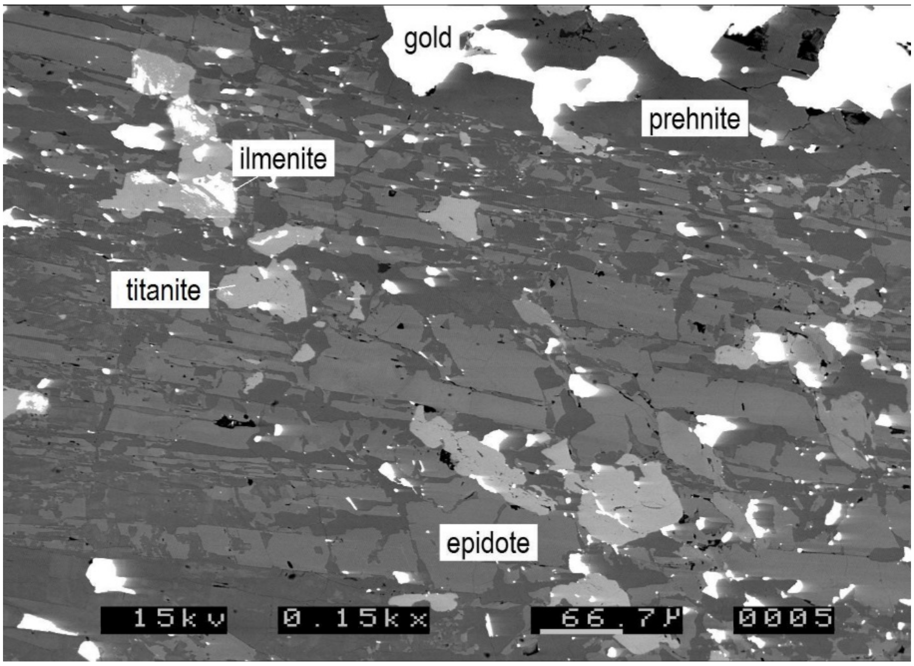

Fig. 5. BSEM image (KD 41 78m) (4/20) Prehnite filling fractures in epidote. Gold hosted by prehnite. Ilmenite partially replaced by titanite.

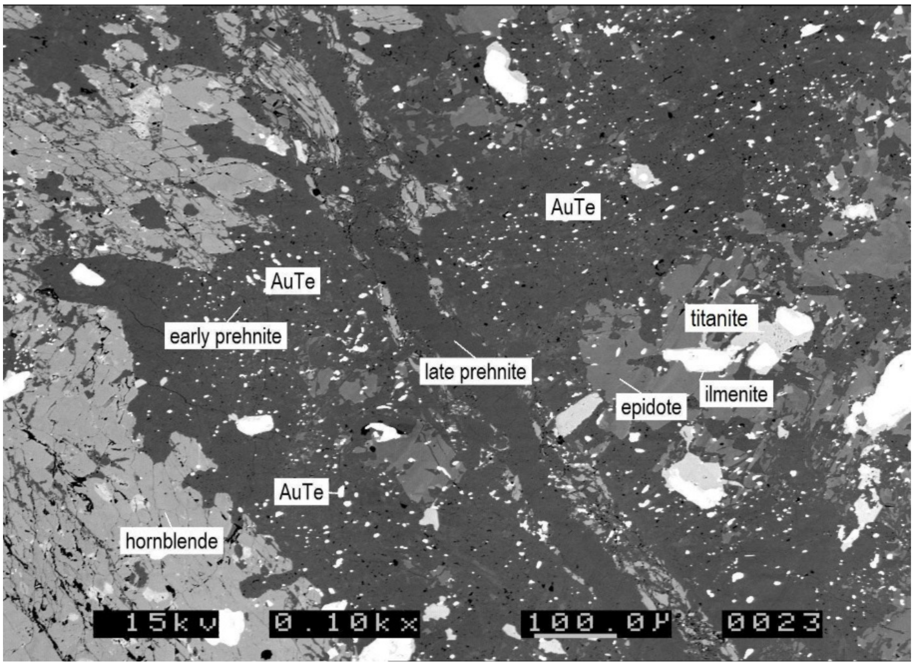

Fig. 6. BSEM image (KD 41 78m) (4/23) Late prehnite occurring in a brittle fracture cutting early prehnite and hornblende. The early prehnite contains numerous small white inclusions of a gold telluride (AuTe), whereas the late prehnite vein is barren. Ilmenite is altered to titanite.

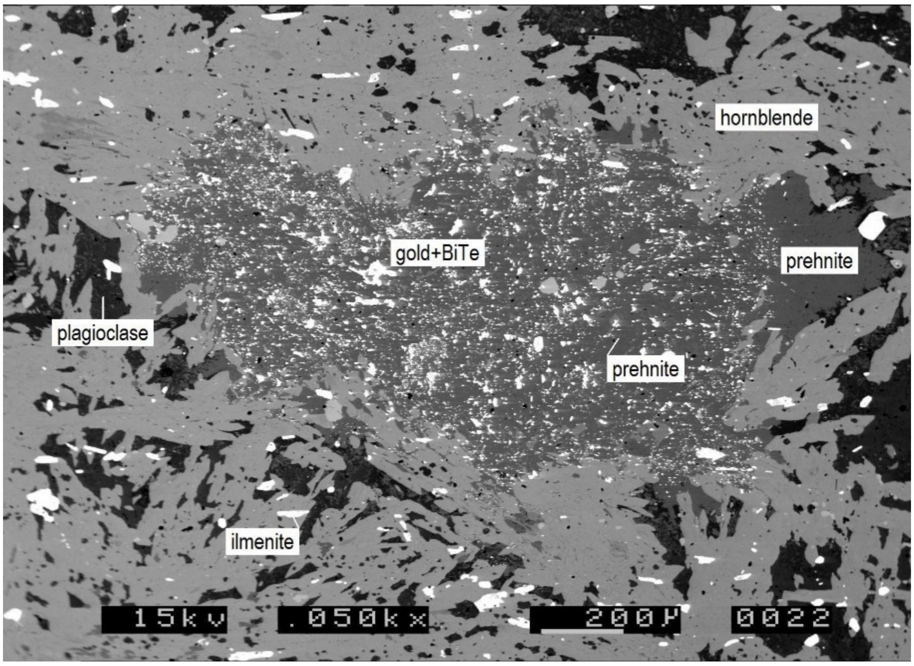

Fig. 7. BSEM image (KD 41 78m) (7/9) Typical `cloud ‘of mineralization hosted by prehnite, which is replacing plagioclase. The white inclusions are mainly gold and tellurobismuthite (BiTe).

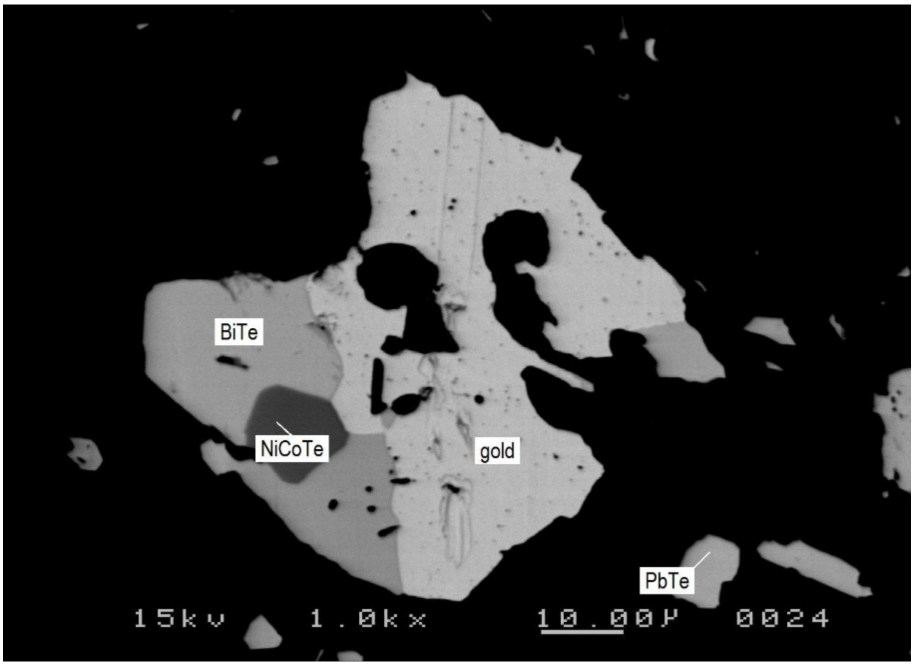

Fig.8. BSEM image (KD 41 78m) (12/2) Composite grain of gold, a bismuth telluride and a nickel cobalt telluride hosted by prehnite. **PbTe = a lead telluride**.

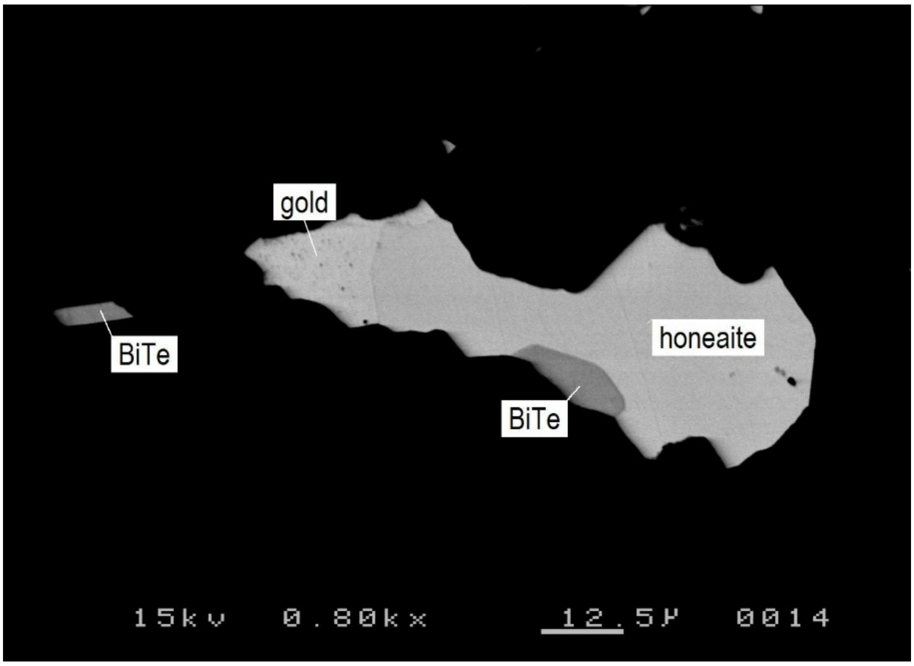

Fig. 9. BSEM image (KD 41 78m) (1/11A) Composite grain of honeaite, a bismuth telluride and gold hosted by prehnite.

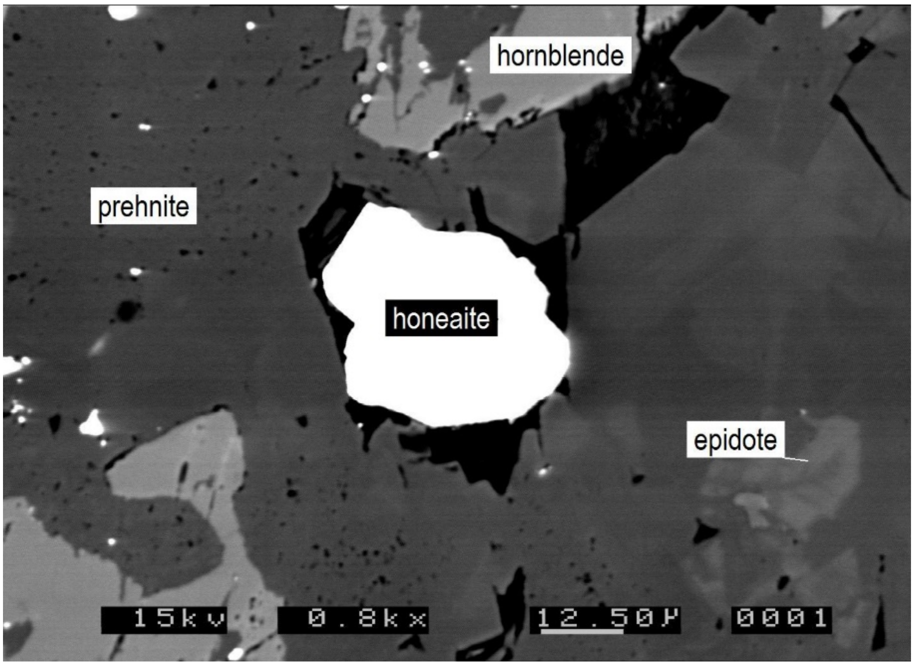

Fig. 10. BSEM image (KD 41 78m) (4/1) Honeaite in vugh within prehnite.

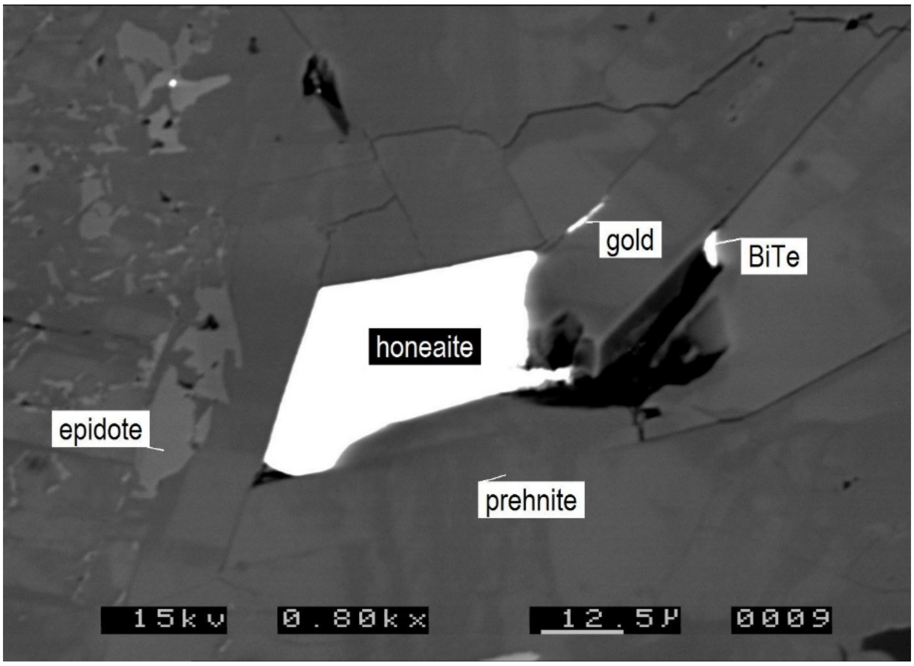

Fig. 11. BSEM image (KD 41 78m) (4/8) Honeaite partially filling cavity in prehnite with a bismuth telluride (BiTe). Gold occurs in a fracture partially exploited by honeaite.

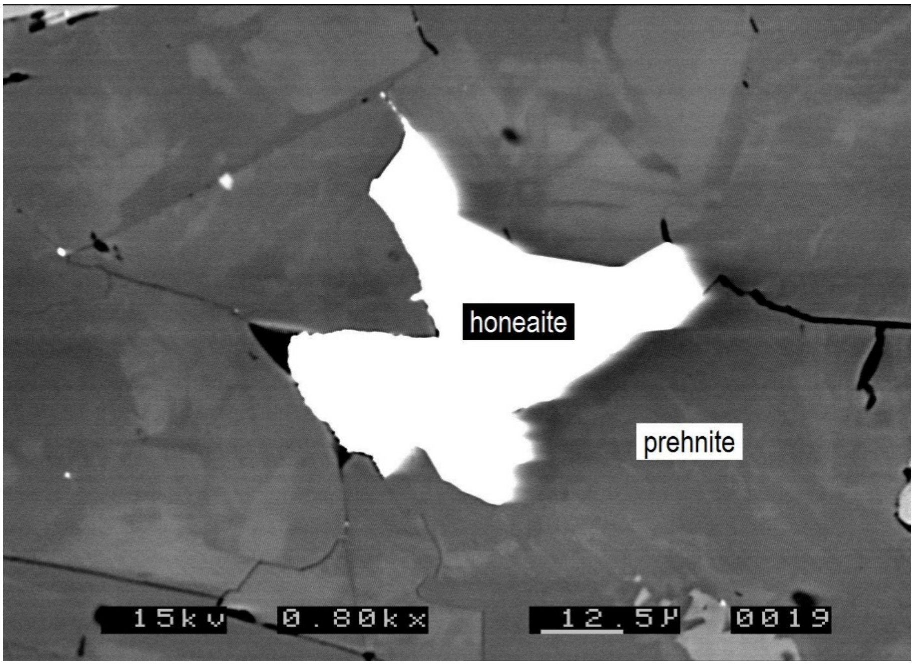

Fig. 12. BSEM image (KD 41 78m) (4/14) Honeaite occurring in cavity in **zoned** prehnite.

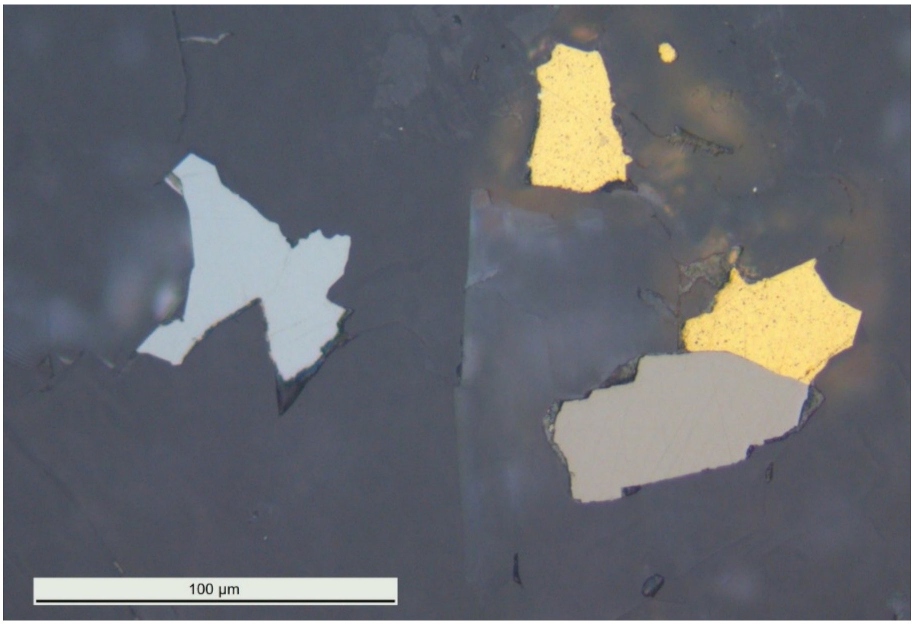

Fig. 13. Reflected light digital image of honeaite (bluish grey) **(same honeaite grain as in fig. 12)**, gold (yellow) and pyrrhotite (brownish-pink) in a gangue of prehnite.

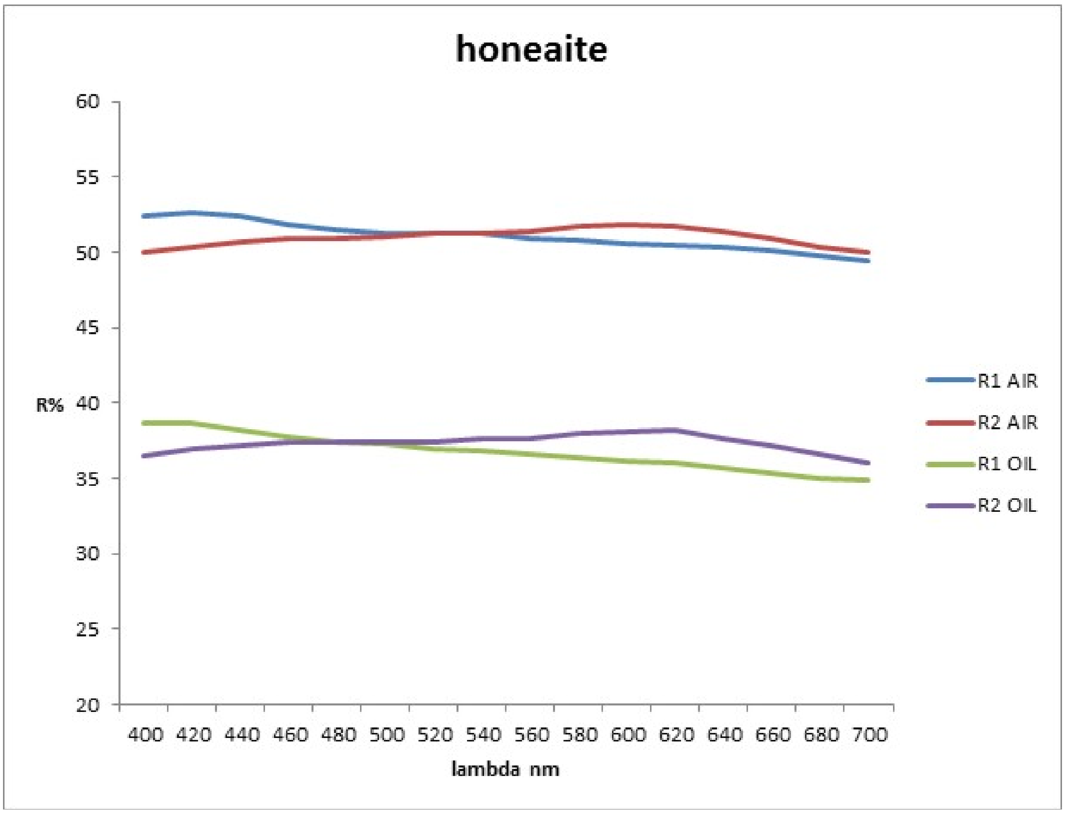

Fig. 14. Reflectance spectra for honeaite

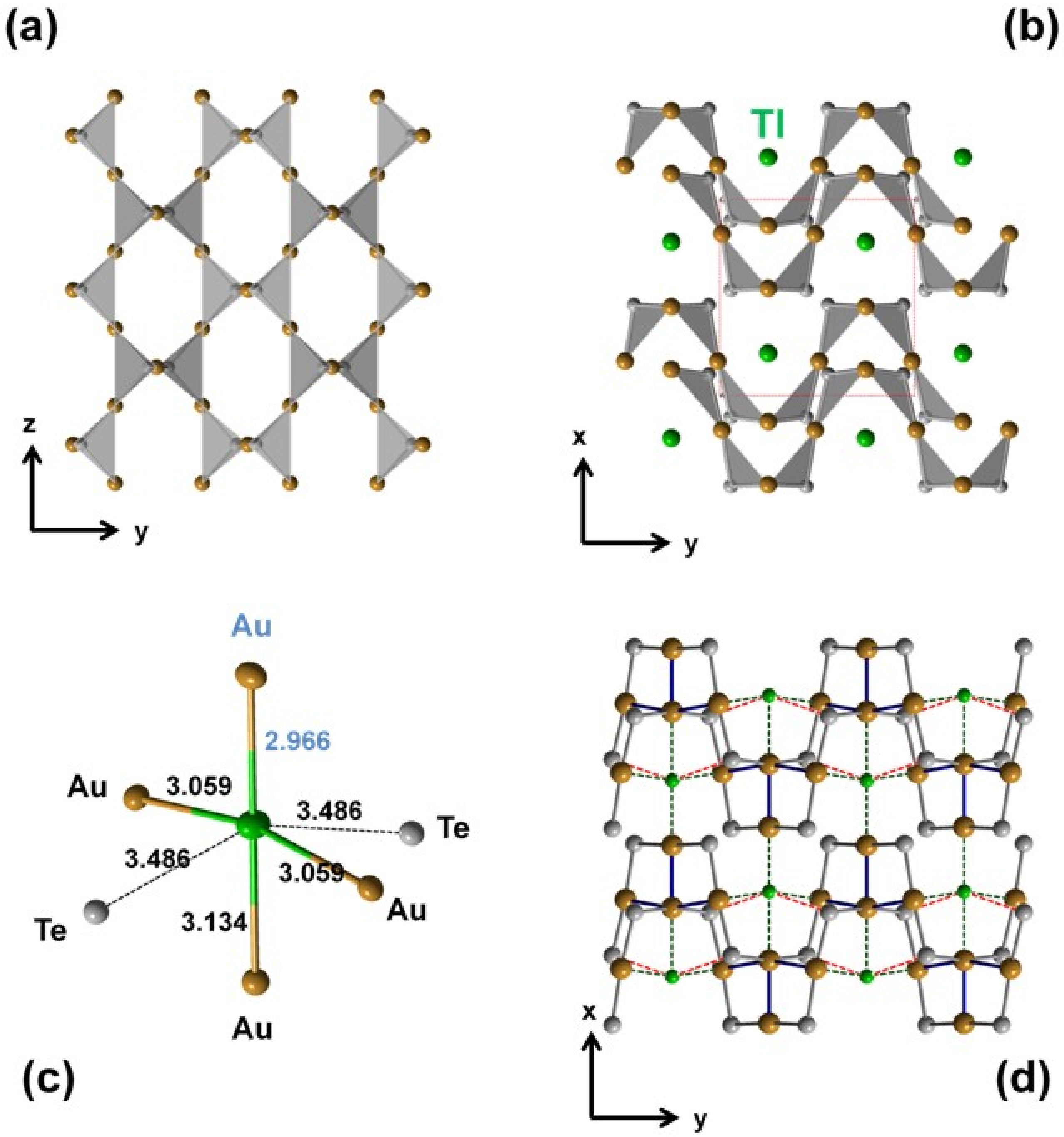

Fig. 15. Crystal structure of honeaite. **(a)** A single corrugated sheet of corner-linked $TeAu_3$ pyramids comprising six-membered rings. **(b)** Full structure showing two double- sheets with $TeAu_3$, pyramids shown in grey. Thallium atoms (green) occur in grooves in the corrugated sheets. The unit-cell projection is shown as a dotted red line. **(c)** Thallium coordination environment in which there are three Tl-Au intra-sheet bonds and a single Tl-Au inter-sheet bond (blue Au label). There are two long Tl···Te intra-sheet distances (dotted lines) that may not be genuine bonds. Numbers are bond distances in Å. **(d)** Ball-and-spoke representation of (b) showing intra-sheet Au-Au bonds (solid blue lines), Tl-Au bonds (black dashed lines) and Tl···Te distances (dashed red lines).

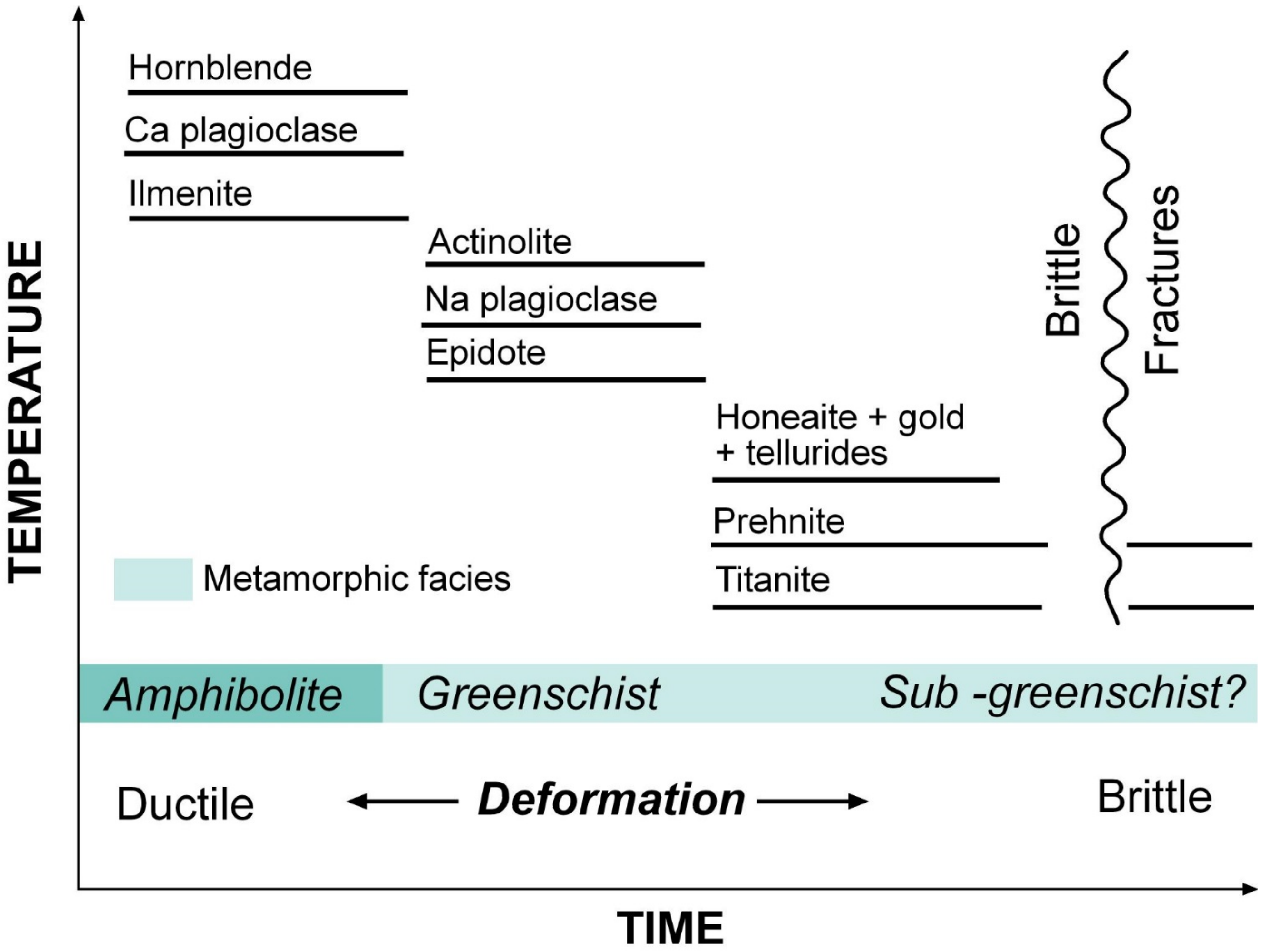

Fig. 16. **The paragenesis** of honeaite.

	Hornblende			Ferro-actinolite		Actinolite		Epidote		Prehnite		Plagioclase			
SiO2	43.74	43.84	43.14	51.59	51.95	54.83	54.25	38.95	38.46	43.43	43.73	60.02	60.23	66.24	65.79
TiO2	0.51	0.53	0.63	0.00	0.00	0.02	0.00	0.00	0.00	0.11	0.02	-	-	-	-
Al2O3	12.48	11.86	12.56	0.88	0.41	0.45	0.61	28.73	25.16	22.22	24.18	25.00	24.82	20.87	21.55
FeO	20.15	20.18	20.30	27.04	26.41	15.80	18.42	-	-	-	-	0.00	0.08	0.17	0.10
Fe2O3	-	-	-	-	-	-	-	6.55	10.23	1.96	0.29	-	-	-	-
MnO	0.33	0.35	0.33	0.35	0.29	0.08	0.26	0.10	0.00	0.01	0.00	-	-	-	-
MgO	7.70	7.88	7.62	5.86	6.92	13.79	12.18	0.10	0.04	0.01	0.01	0.12	0.11	0.17	0.03
CaO	11.65	11.43	11.30	12.11	12.39	12.64	12.63	24.24	23.89	26.55	27.42	6.87	6.76	1.79	2.25
Na2O	1.76	1.63	1.64	0.20	0.21	0.18	0.23	0.02	0.06	0.00	0.02	7.86	7.68	10.27	10.06
K 2O	0.28	0.24	0.31	0.03	0.01	0.00	0.08	-	-	-	-	0.01	0.05	0.17	0.06
Total	98.60	97.94	97.82	98.06	98.58	97.80	98.65	98.69	97.82	94.30	95.66	99.86	99.74	99.68	99.85
O =	**23.00**	**23.00**	**23.00**	**23.00**	**23.00**	**23.00**	**23.00**	**12.50**	**12.50**	**22.00**	**22.00**	**32.00**	**32.00**	**32.00**	**32.00**
Si	6.56	6.62	6.53	7.93	7.93	7.98	7.94	3.00	3.03	6.09	6.01	10.71	10.75	11.66	11.57
Ti	0.06	0.06	0.07	0.00	0.00	0.00	0.00	0.00	0.00	0.01	0.00	-	-	-	-
Al	2.21	2.11	2.24	0.16	0.07	0.08	0.11	2.61	2.34	3.67	3.92	5.26	5.22	4.33	4.47
Fe^{2+}	2.53	2.55	2.57	3.48	3.37	1.92	2.26	-	-	-	-	0.00	0.01	0.03	0.01
Fe^{3+}	-	-	-	-	-	-	-	0.38	0.61	0.21	0.03	-	-	-	-
Mn	0.04	0.05	0.04	0.05	0.04	0.01	0.03	0.01	0.00	0.00	0.00	-	-	-	-
Mg	1.72	1.77	1.72	1.34	1.57	2.99	2.66	0.01	0.00	0.00	0.00	0.03	0.03	0.04	0.01
Ca	1.87	1.85	1.83	1.99	2.03	1.97	1.98	2.00	2.02	3.99	4.04	1.31	1.29	0.34	0.43
Na	0.51	0.48	0.48	0.06	0.06	0.05	0.07	0.00	0.01	0.00	0.01	2.72	2.66	3.51	3.43
K	0.05	0.05	0.06	0.01	0.00	0.00	0.01	-	-	-	-	0.00	0.01	0.04	0.01
Total	15.56	15.53	15.54	15.01	15.07	15.01	15.05	8.01	8.00	13.96	14.01	20.03	19.98	19.95	19.92
											An % =	**32.58**	**32.70**	**8.79**	**11.02**

	Gold		Petzite		Calaverite		Hessite	Tellurobismuthite			Melonite		Mattagamite	Frohbergite
Au	94.30	94.22	25.74	26.17	42.91	42.65	0.00	-	-	**Fe**	0.00	0.09	1.91	15.84
Ag	5.66	5.71	40.45	40.08	0.59	0.60	62.47	-	-	**Co**	4.68	7.25	14.67	1.01
Bi	-	-	-	-	-	-	-	52.38	52.59	**Ni**	12.87	10.48	0.30	0.12
Te	-	-	33.58	33.42	57.09	56.35	38.34	47.36	47.24	**Te**	82.47	82.92	82.83	83.28
Total	99.96	99.93	99.77	99.67	100.59	99.60	100.81	99.74	99.83	**Total**	100.02	100.73	99.71	100.25
		Te =	**2.00**	**2.00**	**2.00**	**2.00**	**1.00**	**3.00**	**3.00**	**Te =**	**2.00**	**2.00**	**2.00**	**2.00**
		Au	0.99	1.01	0.97	0.98	0.00	-	-	**Fe**	0.00	0.00	0.11	0.87
		Ag	2.85	2.84	0.02	0.03	1.93	-	-	**Co**	0.25	0.38	0.77	0.05
		Bi	-	-	-	-	-	2.03	2.04	**Ni**	0.68	0.55	0.02	0.01
		Te	2.00	2.00	2.00	2.00	1.00	3.00	3.00	**Te**	2.00	2.00	2.00	2.00

Table 1. Electron microprobe analyses of Karonie silicates, gold and tellurides

The analyses were carried out using a MICROSCAN MK5 in energy dispersive mode (Link Analytical AN10/25S). The instrumental conditions were: accelerating voltage 15kV, current 2.8 nA, beam diameter c. 5 microns, take off angle 75 degrees and livetime 200 seconds. The standards used are a mixture of natural minerals, metal oxides and pure metals.

Table 2. Reflectance data in air and in oil for honeaite. (COM refers to the Commission on Ore Mineralogy recommended minimum wavelengths)

R_1	R_2	$^{im}R_1$	$^{im}R_2$	λ/nm	R_1	R_2	$^{im}R_1$	$^{im}R_2$	λ/nm
52.4	50.0	38.7	36.5	400	50.9	51.4	36.6	37.7	560
52.6	50.3	38.7	36.9	420	50.8	51.7	36.4	38.0	580
52.5	50.7	38.3	37.2	440	50.7	51.8	36.3	38.0	589 (COM)
51.9	50.9	37.8	37.4	460	50.6	51.9	36.1	38.1	600
51.7	50.9	37.6	37.4	470 (COM)	50.5	51.8	36.0	38.2	620
51.5	50.9	37.4	37.4	480	50.3	51.4	35.7	37.7	640
51.3	51.0	37.3	37.4	500	50.2	51.2	35.5	37.5	650 (COM)
51.3	51.3	36.9	37.4	520	50.1	50.9	35.4	37.2	660
51.2	51.3	36.8	37.6	540	49.8	50.3	35.0	36.6	680
51.1	51.3	36.7	37.6	546 (COM)	49.5	50.0	34.9	36.0	700

Table 3. Electron microprobe analyses of honeaite

Honeaite	Au	Tl	Te	Total
Crystal.1	56.24	19.65	24.40	100.29
Crystal.2	55.82	19.83	24.24	99.88
Crystal.3	56.19	19.45	24.19	99.82
Crystal.4	56.34	19.66	24.25	100.25
Crystal.5	55.91	19.96	24.30	100.16
Crystal.6	56.73	19.49	24.17	100.39
Crystal.7	56.77	19.83	24.38	100.98
Crystal.8	56.43	19.11	24.32	99.86
Crystal.9	56.88	19.86	24.27	101.02
Crystal.10	56.53	20.10	24.22	100.86
Crystal.11	56.47	19.70	24.30	100.47
Crystal.12	56.79	19.23	24.09	100.10
Crystal.13	55.83	19.99	24.59	100.41
Crystal.14	56.61	19.78	24.44	100.83
Crystal.15	55.75	19.82	24.33	99.90
Crystal.16	56.33	19.79	24.34	100.46
Crystal.17	55.98	19.31	24.31	99.60

Constituent	Wt.% (n=17)	Range	Stand. Dev. (1σ)
Au	56.33	55.75-56.88	0.37
Tl	19.68	19.11-20.10	0.27
Te	24.30	24.09-24.59	0.11
Total	100.31		

Standards used for honeaite: Au = Au metal; Tl = Thallium iodide; Te = Te metal. Instrument and operating conditions in Table 1.

Table 4 Calculated powder XRD pattern of honeaite. Only reflections with relative intensities ≥ 5% are shown.

h k l	d_{hkl} (Å)	I/I_{max} (%)
1 1 1	4.915	13
0 2 0	4.438	6
1 2 1	3.547	6
3 0 0	2.989	31
0 2 2	2.938	100
3 1 0	2.833	23
3 1 2	2.296	14
0 4 0	2.219	15
3 2 2, 4 1 1	2.095	47 (39, 8)
0 0 4	1.960	16
3 3 2	1.853	17
3 4 0	1.782	8
3 0 4	1.639	9
3 1 4	1.612	7
0 4 4	1.469	7
3 4 4	1.319	5
6 3 2	1.263	7
0 2 6	1.254	5